ELSEVIER

Chemical Geology 183 (2002) 43–61

CHEMICAL GEOLOGY
INCLUDING
ISOTOPE GEOSCIENCE

www.elsevier.com/locate/chemgeo

Depleted melt inclusions in MORB plagioclase: messages from the mantle or mirages from the magma chamber?

Peter J. Michael [a,*], William F. McDonough [b], Roger L. Nielsen [c], Winton C. Cornell [a]

[a] *Department of Geosciences, The University of Tulsa, 600 S. College Ave., Tulsa, OK 74104, USA*
[b] *Department of Geology, University of Maryland, College Park, MD 20742, USA*
[c] *College of Oceanography and Atmospheric Science Oregon State University, Corvallis, OR 97331, USA*

Abstract

Melt inclusions that are depleted in high field strength elements (HFSE; Ti, Zr, Nb), relative to other incompatible elements, were found in a plagioclase phyric normal mid-ocean ridge basalt (N-MORB) from the southern Mid-Atlantic Ridge. Similar inclusions are present in many other phyric NMORB. HFSE-depleted inclusions constitute only a few percent of all melt inclusions in this sample, and inclusions within individual crystals display a limited range of HFSE-depletion. Relative to host glass, they are depleted in the order: Nb < Zr < Ti ≈ HREE ≈ Th < LREE < U. Concentrations of Si, Al, Fe, Mg and Ca are similar to the host glass. Large ion lithophile elements (LILE) are enriched relative to the host glass in the order: Rb>Ba>K>Pb>Na>Sr. La/Sm is higher than in the host glass. Cl is enriched but not to the level observed in HFSE-depleted inclusions by Nielsen et al. [Geochem. Geophys. Geosyst. (2000) 1], who deemed similar inclusions in other MORB as ''Cl-enriched''. HFSE depletion is not related to inclusion size, plagioclase host composition, or inclusions' Mg#s. Because of the disparate behavior of elements with similar bulk crystal–liquid partition coefficients, the depletion trends cannot be modeled by any process that involves crystal liquid equilibrium, such as melting or crystallization. Nielsen et al. proposed that similar inclusions represent liquids that were formed by melting of hydrothermally altered depleted peridotite. An alternative explanation is that the inclusions' compositions were controlled by diffusional processes. There is a good correlation of the elements' abundance relative to the host with Z^2r_i, a quantity that is highly correlated with diffusion in silicate liquids ([Hofmann, A.W., 1980. Diffusion in natural silicate melts: a critical review. Physics of Magmatic Processes, Princeton Univ. Press, pp. 385–417]; Z = atomic radius and r_i = ionic radius) and possibly in plagioclase. The depletions are consistent with a model in which plagioclase rapidly dissolves to form a plagioclase-like melt, while diffusion through liquid channels or solid plagioclase transports elements from the host liquid to the inclusion. Plagioclase dissolution may have been aided by increased $Cl + H_2O$ in the enclosing magma, which might have been ultimately derived from hydrothermal activity. A second diffusion-related model starts with the entrapment of ultradepleted melt inclusions such as those found in olivine. Subsequent diffusion from a less depleted host melt through solid plagioclase into the inclusion would control the inclusion's incompatible element abundances. Comparison of elements with similar Z^2r_i (e.g., LREE vs. HREE) suggests that the host liquid of the analyzed sample was enriched in incompatible elements despite the inclusions' depletion in Nb, Zr and REE. Compositions of inclusions that are not HFSE-depleted also suggest that the host melt was enriched. Ultradepleted inclusions in MORB olivine [Nature 363 (1993) 151] are not like those in plagioclase: they are depleted in all incompatible elements, and their compositions are

* Corresponding author. Tel.: +1-918-631-3017; fax: +1-918-631-2091.
E-mail address: pjm@utulsa.edu (P.J. Michael).

0009-2541/02/$ - see front matter
PII: S0009-2541(01)00371-0

consistent with progressive fractional melts of the mantle (ibid). However, the possibility of a diffusion relationship should also be examined.

Keywords: Melt inclusion; High field strength elements; MORB plagioclase

1. Introduction

It is widely considered that melt inclusions may isolate early liquids and therefore provide a great deal of information about a magma before it has mixed, coalesced and degassed. The discovery in MORB of inclusions that are ultradepleted in trace elements supports models of fractional melting of the mantle followed by high level mixing (Sobolev, 1996; Shimizu, 1998; Sobolev and Shimizu, 1993; Gurenko and Chaussidon, 1995). A surprisingly wide spectrum of melt compositions are found in inclusions from enriched MORB (E-MORB) and depleted, or normal MORB (N-MORB) suites. Moreover, the entire range of compositional diversity can be found within inclusions from a single crystal (Sobolev et al., 2000; Sobolev and Shimizu, 1993; Nielsen et al., 1995). Mixing of these various melt components, in roughly the proportions that they are observed as inclusions, can generate the trace element characteristics of the host magmas (Sobolev and Shimizu, 1994; Sours-Page et al., 1999).

It may be, however, that the processes involved in inclusion formation may themselves produce some of the compositional diversity seen in these suites. If so, then we need to describe and document the processes involved in inclusion formation in order to explain their diverse compositions before inclusions can be used confidently to understand the diversity of melt sources and melting processes.

In this study, melt inclusions in plagioclase from a primitive N-MORB from the southern MAR (34°S) were analyzed for their major and trace element compositions. Some of the inclusion compositions define an anomalous trend of sharply decreasing abundances of HFSE with constant abundances of LILE. These trends are difficult to explain by processes such as mantle melting and magma mixing. They are consistent with control of trace element concentrations by diffusion through the melt during inclusion formation by crystal melting or by diffusion through plagioclase into an ultradepleted melt. In either case, the inclusions would not provide faithful records of geologically significant magmas that were present in the crust and mantle. The trends are also broadly consistent with transport capabilities of a hydrous fluid, in which case the inclusions might represent unusual but significant magmas from a hydrous, depleted source (Nielsen et al., 2000). The HFSE depletion trends are not unique to this sample; similar trends have been described for melt inclusions in plagioclase from other N-MORB, and were accompanied by high Cl concentrations (Sours-Page et al., 1999; Nielsen et al., 2000). Thus, it is worth considering whether the diversity of inclusion compositions in these suites is a function of their host mineral phase. Moreover, might the encasement processes of other hosts (e.g., olivines) also develop such features?

Our initial intentions were to identify possible end-member mantle components involved in magma mixing, characterize the style of mantle melting, and constrain the timing and sequence of mixing and melting beneath the southern MAR. Our observations have compelled us to examine first local, inclusion-scale processes. This initial investigation will serve as the foundation upon which to characterize the mantle beneath this ridge and also help to establish the role the inclusion formation process plays in controlling trapped melt compositions.

2. Geological setting and sample characteristics

The sample (Plume5 D53-1) is an N-MORB from the center of a 55-km long segment of the Mid-Atlantic Ridge axis at 33°55′S. Although the ridge is immediately south of the most robust and shallow segment along the southern Mid-Atlantic Ridge, this segment is anomalously deep (3400 mbsl) and rifted. The segment spreads at 35 mm/year and is bounded by an oblique offset to the north and the Meteor Transform to the south (Fox et al., 1991; Grindlay et al., 1991).

Host glasses from this segment are all N-MORB and are offset toward high Ba/K at high Ti/K (or high Ba/Nb at high Ti/Nb): a direction that is orthogonal to the trend expected for simple mixing of depleted and enriched components (Fig. 1; Michael et al., 1994). High Ba/Nb and Ba/K values almost certainly reflect the input of a component related to the Tristan da Cunha hotspot (Weaver, 1991), which is about 400 km to the SE. However, the nature of this input is unclear since these MORB are among the most depleted in the region in terms of La/Sm, Zr/Nb, etc. Thus, these observations define the existence of a regional end-member component with high Ba/Nb and Ba/K (like Tristan), and yet with an overall depleted characteristic; this component might itself be a mixture (Michael et al., 1994).

The N-MORB basalt (Plume5 D53-1) with the plagioclase-hosted inclusions has glass with an Mg# of 66.8 and $(La/Sm)_n = 0.42$ (Michael et al., 1994; Michael, unpublished data). Least squares mixing calculations show that P5 D53-1 could serve as the parent liquid to more fractionated compositions from this ridge segment.

The crystals examined (and this petrographic description) are exclusively from the glassy rind of the basalt. The basalt is highly plagioclase phyric, with about 17 modal % plagioclase that ranges from An_{87} to An_{76}. Most of the plagioclase ($\sim$14 modal %) occurs as large (0.3–5 mm) phenocrysts that are sometimes rounded and zoned and usually contain glassy inclusions. The remaining plagioclase occurs as small, elongate phenocrysts and microphenocrysts, 50–500 μm. There is $\sim$2 modal % olivine present, mostly as large (1–2 mm) euhedral phenocrysts, with lesser amounts occurring as small (<200 μm) microphenocrysts. Olivine is observed rarely as large, stress-twinned grains (2 mm), and also as rounded inclusions (about 100 μm) within plagioclase. Spinel is found as dark euhedral grains, 100–200 μm, contained in plagioclase or attached to olivine.

Glassy melt inclusions are contained in plagioclase An_{87-76} and infrequently in olivine. Small inclusions (10–30 μm) are typically spherical to oblate spheroidal, often quite numerous and usually zonally arranged in plagioclase. They typically contain gas or shrinkage bubbles with no internal moving bubbles

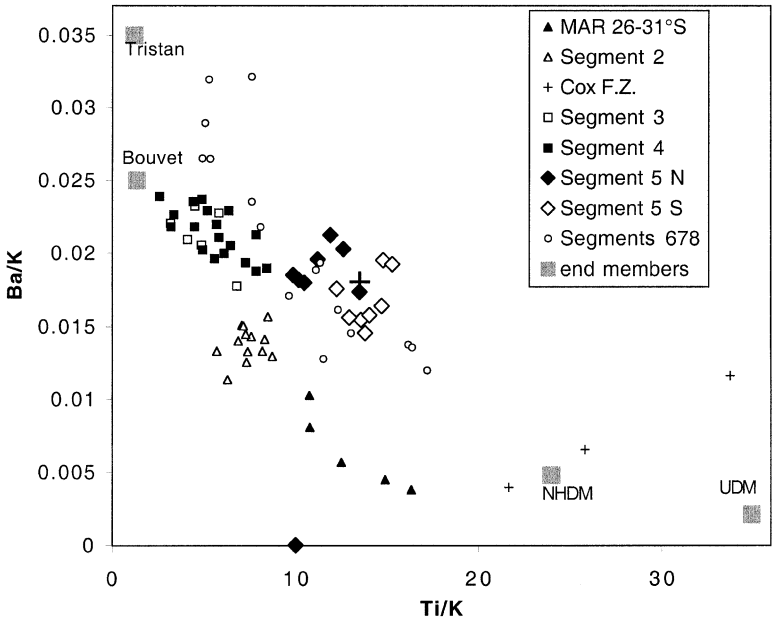

Fig. 1. Ba/K vs. Ti/K for Segment 5: the subject of this study, as well as nearby segments. Separate symbols are shown for the northern and southern portions of Segment 5. All values are ppm elemental ratios. NHDM = Northern Hemisphere depleted mantle. UDM = a model ultradepleted mantle. Large cross denotes sample D53-1, the host MORB glass of this study. High Ti/K is depleted, low Ti/K is enriched. Mixing on this diagram occurs as straight lines. The offset of Segment 5's arrays toward high Ba/K and Ti/K are anomalous.

Table 1
Comparison of LA-ICP-MS (Harvard) with solution ICP-MS (Oregon State Univ.)

Sample no.	P5 D53-1	P5 D70-4	P5 35-1	P5 D59-1	P5 D41-1	P5 D31-2	P5 D54-2
Ti 49	6800	7915	9957	8411	8055	13904	8769
LA	5875	7014	8573	7194	7014	12709	7853
Ni 60	133.0	113.1	136.6	159.9	86.7	64.6	93.1
LA	140.0	122.0	152.0	149.0	92.0	80.0	98.0
Rb 85	0.73	1.19	4.12	1.33	2.81	6.56	0.91
LA			5.00		2.70	7.00	
Sr 86	89.5	133.5	141.3	97.7	142.5	167.2	113.6
LA	86.0	129.0	133.0	90.0	133.0	161.0	107.5
Y 89	26.5	29.2	34.0	34.1	28.7	55.4	36.0
LA	23.7	25.8	28.0	27.6	24.0	47.5	30.0
Zr 90,91	61.9	89.9	113.3	90.7	88.0	211.9	92.9
LA	52.0	80.2	93.0	74.8	76.0	195.5	83.0
Nb 93	1.37	2.89	9.19	2.41	5.79	12.19	1.76
LA	1.16	2.26	6.95	1.95	4.68	9.47	1.55
Ba 135, 136	9.2	13.5	45.7	13.5	33.1	57.3	10.7
LA	9.8	13.7	43.0	13.1	32.0	52.6	10.6
La 139	1.75	3.42	6.92	2.99	4.82	10.31	2.65
LA	2.02	3.62	6.79	2.90	4.98	10.79	2.86
Ce 140	5.62	10.26	16.88	9.23	12.57	27.53	9.18
LA	5.89	10.20	15.86	8.74	12.00	27.00	9.00
Pr 141	1.01	1.64	2.51	1.68	1.90	4.20	1.66
LA	1.05	1.58	2.20	1.97	1.81	3.87	1.60
Nd 146	5.87	9.07	12.11	9.02	9.77	20.32	9.30
LA	6.22	8.99	11.71	8.65	9.15	20.42	8.85
Sm 147, 149	2.51	3.12	3.92	3.27	3.12	6.52	3.32
LA	2.45	2.99	3.42	3.00	3.00	6.25	3.33
Eu 151, 153	0.86	1.031	1.222	1.107	1.064	1.90	1.15
LA	1.00	1.170	1.280	1.110	1.070	2.15	1.21
Gd 157, 158	2.84	3.43	4.29	3.79	3.50	7.38	4.39
LA	3.38	3.89	4.32	3.87	3.47	7.07	4.32
Tb 159	0.62	0.710	0.853	0.742	0.694	1.42	0.87
LA	0.63	0.705	0.785	0.770	0.655	1.32	0.82
Ho 165	0.89	1.00	1.21	1.15	1.02	1.79	1.21
LA	0.95	1.01	1.11	1.06	0.95	1.85	1.14
Tm 169	0.410	0.462	0.510	0.515	0.446	0.866	0.532
LA	0.360	0.387	0.445	0.433	0.365	0.745	0.480
Yb 172, 174	2.45	2.80	3.19	3.11	2.73	4.86	3.25
LA	2.47	2.81	2.99	3.02	2.65	5.00	3.46
Lu 175	0.378	0.423	0.475	0.486	0.419	0.768	0.468
LA	0.370	0.385	0.445	0.426	0.375	0.750	0.435
Hf 177, 178	1.71	2.14	2.76	2.28	2.19	5.11	2.46
LA	1.60	2.14	2.39	2.13	1.96	4.84	2.30
Ta 181	0.109	0.466	0.752	0.220	0.562	0.723	0.138
LA	0.070	0.140	0.395	0.113	0.260	0.525	0.095
Pb 206, 207	0.388	0.571	0.869	0.544	0.677	1.111	0.564
LA	0.392	0.550	0.617	0.453	0.565	1.160	0.485
Th 232	0.088	0.182	0.535	0.164	0.398	0.812	0.107
LA	0.100	0.190	0.648	0.166	0.415	0.880	0.135
U 238	0.017	0.064	0.189	0.035	0.115	0.284	0.018
LA	0.033	0.074	0.209	0.054	0.14	0.37	0.059

Analyses in first row for each element are by solution ICP-MS.
Analysis in second row for each element are LA = Laser ablation ICP-MS.

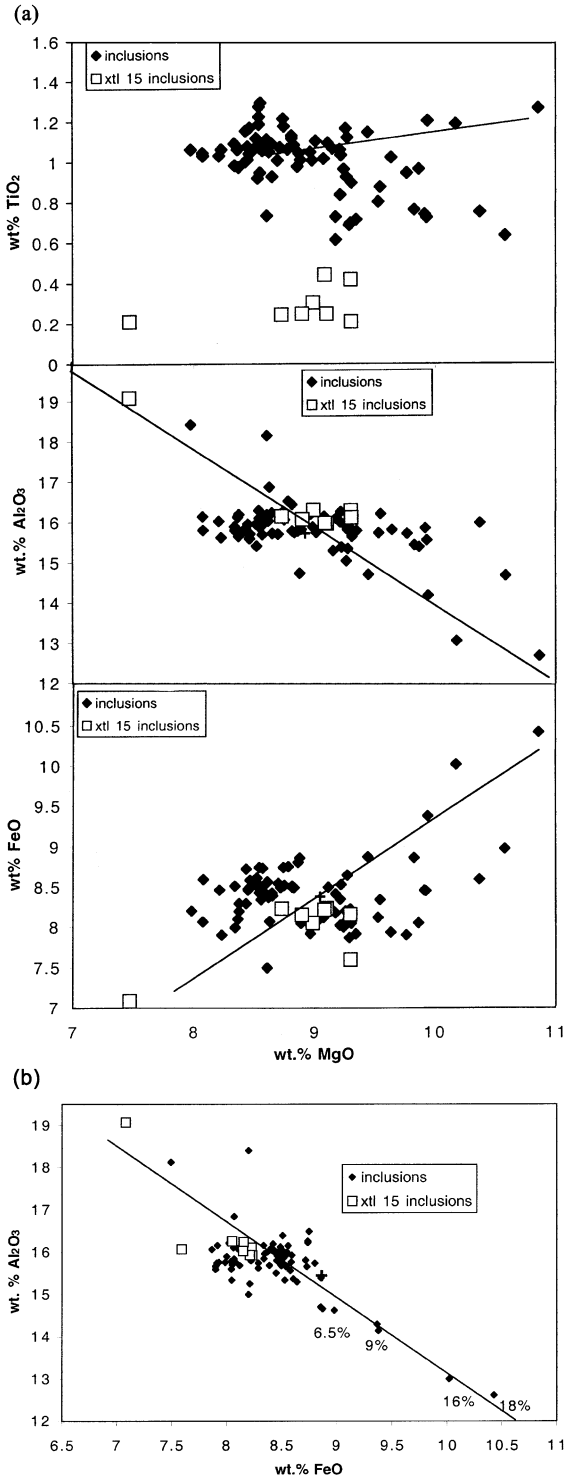

observed. Large inclusions, up to 300 μm in diameter, may be round or elongated or irregular and patchy in shape. Large inclusions of any shape may occur in the same crystal with small inclusions. Patchy, irregular inclusions often seem to be darker and may be devitrified, and many do not have shrinkage bubbles. Most of the analyzed inclusions are large and either spherical or oblate spheroidal, with a shrinkage bubble.

3. Analytical methods

The glassy selvage was removed from the basalt, gently crushed in a steel mortar and sieved to a coarse sand size. Some breakage of crystals occurred during this procedure. Crystals were separated from glass using a Franz® Isodynamic magnetic separator followed by hand picking under a binocular microscope. Twenty-two crystals were selected for mounting and analysis based on the presence of abundant, large and glassy melt inclusions. Crystals were mounted in thermoplastic cement and ground to expose inclusions. When melt inclusions were optimally exposed for an individual crystal, that crystal was removed and placed in an epoxy mount.

Melt inclusions and host plagioclase were analyzed for major element contents using the fully automated WDS Cameca MBX microprobe at The University of

Fig. 2. (a) MgO variation diagrams for plagioclase-hosted inclusions from sample Plume 5 D53-1. All values are expressed in wt.% oxide. Open squares denote the most HFSE-depleted inclusions and are all from a single crystal (#15). Filled diamonds are for all other inclusions, including some that are mildly HFSE-depleted. The thin line is a plagioclase control line estimated from the densest cluster of inclusions. A few (six) inclusions that plot near the line toward higher MgO contents have suffered post-entrapment crystallization as determined in (b). These inclusions were not analyzed for trace elements and do not appear in Figs. 4–7. Points with the lowest MgO contents have also suffered analytical problems (electron beam overlap on host plagioclase). The rest of the inclusions define a trend of constant Al_2O_3, and increasing FeO and TiO_2 with decreasing MgO. The cross denotes the host glass, P5 D53-1. (b) FeO vs. Al_2O_3: symbols and line as in (a). For the line, higher FeO and lower Al_2O_3 denote post-entrapment plagioclase crystallization. All values are expressed in wt.% oxide. The numbers 6.5%, 9%, 16% and 18% next to points show the amount of post-entrapment crystallization that could account for the FeO and Al_2O_3 contents, assuming crystallization of plagioclase having 32% Al_2O_3 and 0.5% FeO from an inclusion having 16% Al_2O_3 and 8.5% FeO.

Table 2
Major element concentrations of plagioclase-hosted melt inclusions in Plume5 D53-1 (all concentrations in wt.%)

Crystal	Inclusion	SiO_2	TiO_2	Al_2O_3	FeO	MnO	MgO	CaO	Na_2O	K_2O	P_2O_5	Total	Inclusion size (μm)		Cl (ppm)
1	2	48.82	1.12	12.55	11.08	0.21	10.84	10.00	1.81	0.166	0.05	96.65			
2	1	51.37	1.07	15.92	8.54	0.16	8.52	11.35	2.92	0.096	0.13	100.06	40	80	
2	3	50.83	1.07	16.00	8.55	0.12	8.60	11.04	3.12	0.116	0.13	99.57	30	30	
2	4	51.25	1.00	15.75	8.29	0.16	8.43	11.26	2.87	0.116	0.10	99.22	40	40	
2	6	50.53	1.29	15.85	8.34	0.14	8.55	11.60	2.84	0.076	0.13	99.35	100	100	38
2	7	51.63	1.09	16.00	8.37	0.16	8.62	11.21	3.02	0.112	0.07	100.28	30	50	34[a]
2	9	50.54	1.26	12.61	10.43	0.20	10.86	11.53	2.31	0.107	0.14	99.99	10	20	
2	10	50.58	1.09	15.86	8.51	0.11	8.34	11.54	2.79	0.101	0.09	99.00	60	80	
2	11	50.66	1.27	15.86	8.52	0.14	8.54	11.38	2.85	0.103	0.10	99.43	60	120	
2	12	50.07	1.04	15.68	8.50	0.18	8.46	11.20	3.13	0.131	0.11	98.51	25	40	
2	13	50.92	1.01	15.92	8.46	0.12	8.45	11.59	2.87	0.102	0.08	99.52	50	70	
2	16	50.44	1.03	15.77	8.59	0.24	8.08	11.40	2.65	0.111	0.10	98.41	70	70	
3	1	50.88	0.76	15.39	8.86	0.18	9.83	11.27	2.68	0.083	0.07	100.00	60	100	
3	3	50.84	0.63	14.62	8.98	0.21	10.58	10.50	2.26	0.115	0.03	98.77	15	15	
3	5	52.30	0.65	14.29	9.37	0.25	11.12	11.09	2.84	0.110	0.01	102.03	15	15	
4	1	51.64	1.19	16.13	8.63	0.21	8.74	11.61	2.81	0.092	0.14	101.18	50	35	
4	2	50.87	1.17	16.00	8.62	0.12	8.68	11.78	2.65	0.100	0.10	100.09	80	100	
4	3	50.06	1.13	15.59	8.66	0.15	8.47	11.38	2.54	0.113	0.09	98.19	30	30	51
4	4	49.36	1.06	18.40	8.20	0.20	7.98	10.92	2.87	0.096	0.10	99.18	50	40	
4	5	51.69	1.02	16.11	8.78	0.14	8.82	11.60	2.82	0.114	0.10	101.19	20	20	
5	1	52.21	1.05	16.16	7.92	0.12	8.97	11.42	2.70	0.077	0.15	100.76	60	70	
6	1	51.59	1.13	16.40	8.51	0.23	8.81	11.57	2.77	0.123	0.13	101.26	50	70	
6	2	50.51	1.06	16.16	8.19	0.16	8.37	11.43	2.78	0.104	0.13	98.90	100	100	
6	3	50.88	1.09	16.03	8.43	0.17	8.58	11.77	2.85	0.088	0.14	100.04	120	150	
6	4	50.69	1.18	16.06	8.43	0.24	8.54	11.65	2.69	0.089	0.14	99.71	50	50	
6	5	50.25	0.94	16.09	8.41	0.19	8.55	11.31	3.05	0.106	0.11	99.00	40	40	
6	7	51.17	1.09	16.20	8.42	0.17	8.65	10.96	3.12	0.108	0.11	99.99	20	20	
6	8	51.08	1.14	14.66	8.87	0.39	9.45	10.93	2.76	0.130	0.09	99.50	15	15	
7	1	51.16	1.07	15.92	8.47	0.16	8.45	11.67	2.62	0.089	0.12	99.73	20	70	
7	2	50.90	1.06	15.96	8.34	0.17	9.21	11.71	2.59	0.078	0.11	100.14	30	100	
7	3	50.91	1.06	16.09	8.10	0.21	8.36	11.26	2.77	0.097	0.12	98.99	50	120	
7	5	51.02	1.01	15.66	8.54	0.17	8.70	11.30	2.98	0.106	0.06	99.55	10	15	
8	1	51.34	0.87	16.16	8.34	0.20	9.55	11.77	2.89	0.057	0.10	101.28	30	60	
9	1	50.92	1.05	16.84	8.07	0.21	8.63	11.79	2.75	0.051	0.12	100.42	15	15	
10	1	50.96	0.84	16.22	8.02	0.20	9.22	11.44	2.79	0.078	0.08	99.84	50	120	
10	2	50.15	0.68	16.06	7.87	0.16	9.29	11.55	2.83	0.073	0.07	98.74	40	50	
10	3	52.05	0.61	16.05	8.41	0.16	9.18	11.30	2.86	0.099	0.06	100.78	15	15	
11	1	50.30	0.72	16.05	8.18	0.21	9.18	11.70	2.68	0.076	0.10	99.20	250	250	b.d.
11	2	44.21	0.73	18.13	7.50	0.16	8.61	9.65	2.02	0.104	0.05	91.16	20	20	
11	3	49.32	0.69	15.80	8.22	0.19	9.30	11.14	2.62	0.103	0.09	97.48	40	40	
11	4	51.85	0.74	15.80	8.46	0.20	9.92	11.06	2.77	0.099	0.10	101.00	20	15	
11	5	50.90	0.72	15.51	8.45	0.24	9.93	11.28	2.63	0.092	0.06	99.82	40	40	37
11	6	51.57	0.75	15.93	8.59	0.28	10.37	10.89	2.72	0.102	0.08	101.28	25	25	
12	1	51.00	1.11	16.15	8.56	0.22	8.61	11.74	2.91	0.100	0.13	100.53	150	150	
12	2	51.36	1.07	16.12	8.49	0.21	8.72	11.73	2.82	0.100	0.12	100.74	200	300	
12	3	50.00	1.03	16.00	8.46	0.20	8.21	10.88	2.57	0.142	0.13	97.62	20	20	
13	1	50.90	1.01	16.10	8.12	0.18	9.08	11.76	2.83	0.067	0.11	100.17	80	50	
14	1	50.50	0.99	15.80	8.03	0.17	8.66	11.61	2.68	0.093	0.11	98.66	100	400	
14	2	50.31	1.06	15.59	7.90	0.15	8.23	11.38	2.97	0.087	0.16	97.84	30	20	
15	1	52.47	0.24	16.11	8.23	0.22	8.73	11.34	2.89	0.104	0.00	100.32	60	70	89
15	2	52.32	0.25	15.93	8.23	0.23	9.10	11.21	2.76	0.112	0.02	100.16	30	40	
15	3	51.84	0.21	19.07	7.08	0.17	7.47	12.45	2.83	0.078	0.00	101.20	30	40	

Table 2 (*continued*)

Crystal	Inclusion	SiO_2	TiO_2	Al_2O_3	FeO	MnO	MgO	CaO	Na_2O	K_2O	P_2O_5	Total	Inclusion size (μm)		Cl (ppm)
15	5	52.18	0.30	16.26	8.05	0.16	8.99	11.23	2.90	0.090	0.00	100.17	50	70	65
15	0	51.67	0.42	16.24	8.16	0.16	9.30	11.24	2.92	0.100	0.01	100.21	200	200	32
15	7	51.89	0.21	16.08	7.59	0.17	9.30	11.13	2.84	0.133	0.04	99.38	25	25	45
15	8	50.52	0.44	15.93	8.21	0.17	9.08	11.54	2.96	0.092	0.01	98.96	25	25	17
15	14	51.81	0.25	16.03	8.15	0.10	8.90	11.16	2.70	0.095	0.00	99.19	25	25	12
16	1	50.25	0.92	15.77	8.08	0.19	9.27	11.73	2.52	0.065	0.09	98.89	240	150	
16	2	51.34	0.80	15.69	8.12	0.12	9.53	11.76	2.40	0.071	0.11	99.93	100	100	
17	1	51.54	1.09	15.94	8.50	0.13	9.11	11.91	2.43	0.070	0.10	100.81	100	200	
17	2	50.69	1.05	15.66	8.73	0.24	8.57	11.55	2.50	0.103	0.11	99.21	20	30	
18	1	50.50	1.17	15.56	8.58	0.19	8.46	11.64	2.64	0.097	0.11	98.95	100	100	
18	3	50.00	0.97	15.62	8.29	0.18	8.37	10.88	2.58	0.110	0.12	97.13	30	50	
18	4	50.71	1.10	15.50	8.57	0.17	9.05	11.82	2.39	0.082	0.12	99.51	100	120	
18	5	50.46	1.04	14.70	8.86	0.21	8.87	10.97	2.47	0.103	0.15	97.84	80	80	
20	1	51.58	0.92	15.96	8.49	0.16	8.53	11.38	2.83	0.106	0.13	100.08	40	50	
20	2	50.50	1.18	12.99	10.02	0.23	10.18	11.39	2.23	0.098	0.15	98.98	40	60	
20	3	50.62	1.03	15.34	8.53	0.17	9.22	11.26	2.68	0.096	0.13	99.09	70	70	
20	6	50.63	1.20	14.14	9.38	0.15	9.94	10.93	2.48	0.110	0.15	99.11	25	25	
20	7	50.51	0.93	15.69	8.39	0.20	8.65	11.15	2.66	0.116	0.12	98.42	30	40	
21	1	50.83	0.89	15.60	8.04	0.13	9.31	11.81	2.58	0.042	0.14	99.38	120	90	
21	2	51.52	0.71	15.74	7.91	0.14	9.35	11.50	2.46	0.057	0.07	99.45	30	20	
22	1	50.10	0.94	15.66	7.90	0.17	9.77	11.46	2.31	0.030	0.11	98.45			
22	2	49.90	0.96	15.34	8.05	0.18	9.87	11.40	2.49	0.045	0.09	98.33			
22	3	50.15	1.02	15.76	7.93	0.19	9.64	11.53	2.52	0.010	0.09	98.84			
23	1	49.78	0.96	15.90	8.00	0.18	9.24	11.51	2.83	0.093	0.10	98.61	150	150	
23	2	50.04	1.10	15.71	8.05	0.11	9.01	11.27	2.48	0.105	0.10	97.99	30	30	
23	3	49.97	1.01	15.79	8.04	0.16	8.89	11.70	2.48	0.097	0.09	98.22	60	60	
23	4	50.12	1.06	15.25	8.21	0.12	9.15	11.53	2.59	0.048	0.06	98.15	140	120	
23	5	50.08	1.16	15.00	8.20	0.18	9.26	11.28	2.76	0.048	0.07	98.03	30	30	

Inclusion size (two columns) show length and width of oblate spheroid.

[a] Cl analyzed on an adjacent inclusion: for crystal #15, five additional Cl analyses are 12, 18, 30, 30, 74 ppm.

Tulsa. Accelerating voltage was 15 kV, beam current was 15 nA, and counting times ranged from 10 to 80 s. Beam diameter was 10 μm, sufficiently small to avoid the surrounding feldspar during inclusion analysis. Natural mineral and glass standards were used. To account for instrument drift, glass analyses are normalized to Hawaiian basaltic glass and Kakanui augite (Jarosewich et al., 1980) run concurrently with the samples. Glass analyses are either single spot analyses or the average of two or three spots. Multiple spot analyses of individual inclusions indicate that they are generally homogeneous. Host plagioclase crystals were analyzed using similar methods. Selected inclusions were analyzed for Cl and S contents using similar conditions but longer counting times (800 s/spot).

Selected melt inclusions >20 μm in diameter were analyzed by laser ablation inductively coupled plasma mass spectrometry (LA-ICPMS) using a procedure similar to that outlined in Rudnick et al. (2000). The laser ablation unit is the DUV (Merchantek/New Wave Research), which uses an ArF excimer laser operating at 193 nm to achieve ablation. A helium jet flow transports the ablated effluent from the sample cell to the mass spectrometer. Low laser energy was used in order to remove $\sim$50 nm layers with each laser pulse; thus, at a 10 Hz repetition rate, most inclusions were consumed at a rate of $\sim$0.5 μm/s. The laser ablation system was coupled to a quadrupole ICPMS (i.e., VG PQ2+). The analyses were accumulated in pulse counting mode, 1 point/peak, with 10 ms dwell times and 5 ms settling times. The

analyses of NIST 610 or NIST 612 before and after a series of inclusion analyses provided for calibration and drift corrections. The preferred values used for the NIST glass compositions were those reported in Pearce et al. (1997). In all cases, Ti was used as an internal standard element for data processing. Comparison of LA-ICPMS analyses with solution ICPMS analyses of host glasses done by the method described in Pyle et al. (1995) in Table 1 shows that the methods yield comparable results for most elements.

4. Post-entrapment crystallization of plagioclase

The inclusions were *not* heated to re-equilibrate their major element compositions. Some of the chemical trends seen in Fig. 2 indicate that several melt inclusions' compositions are affected by post-entrapment crystallization. A small number of the inclusions have higher MgO, FeO and TiO_2, and lower Al_2O_3 when compared to the bulk of the inclusions (Table 2; Fig. 2). This is due to post-entrapment plagioclase crystallization since it follows closely along plagioclase control lines (Fig. 2a). The affected inclusions are typically (but not always) smaller than 25 μm in size (Table 2). The amount of crystallization can be estimated by assuming that the affected inclusions

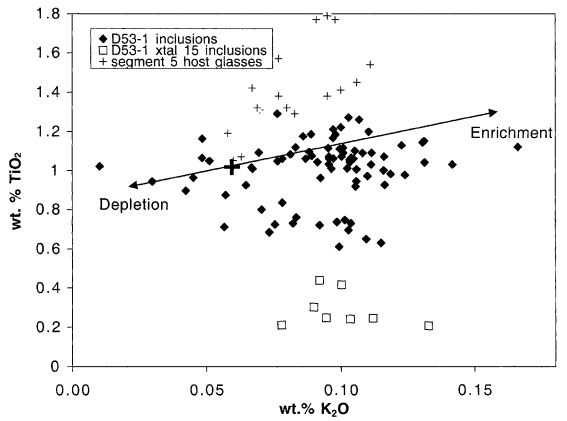

Fig. 3. K_2O vs. TiO_2. All values are expressed in wt.% oxide. Symbols as in Fig. 2, except addition of crosses which represent other bulk glasses from Segment 5. The large cross shows the composition of the host glass of this study. Line with arrows shows the trend expected for magmatic enrichment or depletion which should project to the TiO_2 axis. Note HFSE-depleted inclusions are displaced below and orthogonally from this trend.

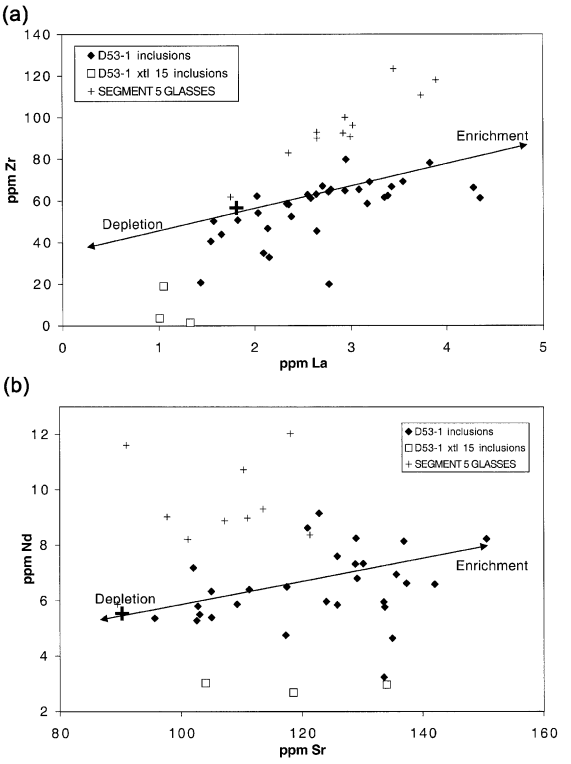

Fig. 4. (a) Zr vs. La, and (b) Nd vs. Sr for inclusions. All values are expressed in ppm. Symbols as in Figs. 2 and 3. Line with arrows shows the general trend expected for magmatic enrichment or depletion assuming that La is more incompatible than Zr, and Sr is more incompatible than Nd. Note that HFSE-depleted inclusions are displaced nearly orthogonally from these trends. No inclusions that have suffered from significant post-entrapment crystallization or laser overlap on plagioclase are included here.

were initially similar to the other inclusions and then crystallized plagioclase of approximately the same composition as the host. The most strongly affected inclusions with FeO $\sim$10.5% and Al_2O_3 $\sim$12.5% underwent about 18% crystallization (Fig. 2b). There are only two inclusions that show >10% post-entrapment crystallization, and most show much less. The process affects the major element compositions of inclusions, so these must be viewed with some caution. The Mg# is unaffected, however, so it is used in latter diagrams instead of MgO when examining other processes. Most incompatible element ratios are unaffected, although ratios involving Sr and Eu will be changed due to plagioclase crystallization. Incompatible element concentrations are only slightly affected

because the amount of crystallization is small. A few small inclusions fall on the plagioclase control line at lower FeO and higher Al_2O_3 (Fig. 2). These analyses almost certainly reflect electron beam overlap on the host plagioclase.

5. Depletion related to ionic field strength

A few inclusions have compositions that display notable deviations from that of the host glass (Tables 2 and 3). Compared to the host glass and most other inclusions, they are strongly depleted in HFSE, less depleted in rare earth elements (REE), and not depleted in LILE. Henceforth, this is termed HFSE depletion. Fortunately, the distinctive HFSE depletion is expressed consistently and strongly in the inclusions of one particular crystal, which are plotted in all diagrams using a separate symbol for purposes of comparison. This HFSE depletion is also expressed to a lesser degree in a few inclusions from other crystals, but appears to be absent in most inclusions. In this suite, unlike some earlier studies (Nielsen et al., 1995), each crystal displays a very limited range of HFSE depletion compared to the entire suite of inclusions, suggesting that most, if not all, of the inclusions that were analyzed within a crystal formed during a short time interval.

The HFSE depletion is immediately apparent in the larger data set of major elements, in a plot of K_2O vs. TiO_2 (Fig. 3). The trends are not simply the depletion of all incompatible elements since K_2O is not depleted. Whenever a higher field strength element is plotted against a lower field strength element, e.g., REE vs. LILE, HFSE vs. REE, HFSE vs. LILE (Fig. 4a and b), the concentration of the ion with the higher field strength (i.e., charge/radius) decreases more rapidly as seen in the low-Ti inclusions, approaching zero. This is also apparent in diagrams involving ratios of elements with different field strengths (Fig. 5a and b). The HFSE-depleted inclusions have slightly elevated levels of Cl (80 ppm) compared to the host glass (15 ppm) and the other inclusions (30 ppm) (Table 3). The Cl enrichment is too mild and the number of analyses is too small to define a trend of increasing Cl with decreasing HFSE, as was shown by Nielsen et al. (2000) for inclusions from several suites of MORB with greater Cl enrichment.

HFSE-depleted inclusions have been seen in other MORB plagioclase as well (Nielsen et al., 2000; Sours-Page et al., 1999), but the inclusions were not described as HFSE-depleted in these earlier studies, partly because the most Ti-depleted inclusions tended to also have high MgO contents (and Mg#s). The inclusions in this study display a range of Mg#, and there is no correlation of HFSE depletion with Mg#. In any case, the similarity of HFSE depletion in inclusions from several widely separated samples shows that whatever process causes the HFSE deple-

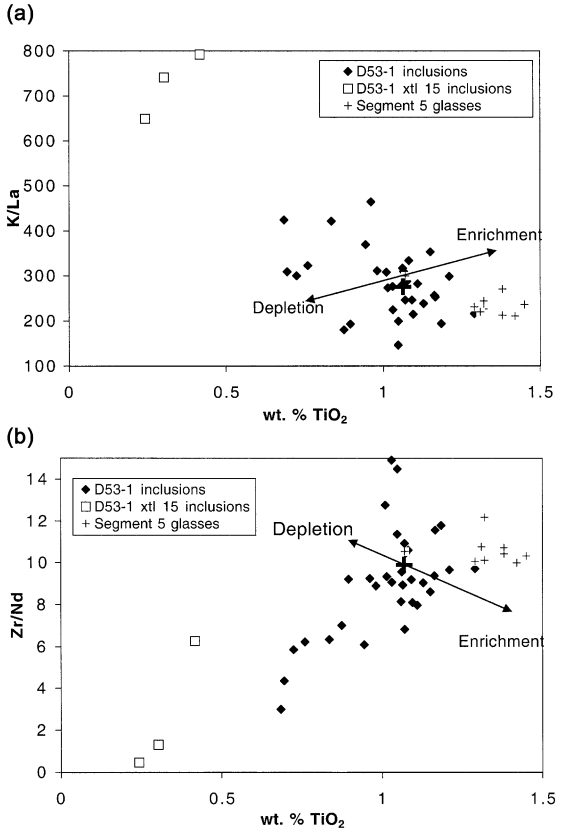

Fig. 5. (a) Wt. % TiO_2 vs. K/La, and (b) wt.% TiO_2 vs. Zr/Nd for inclusions. Symbols as in Figs. 2 and 3. Line with arrows shows the general trend expected for magmatic enrichment or depletion assuming that K is more incompatible than La, and Nd is more incompatible than Zr. Note HFSE-depleted inclusions are displaced nearly orthogonally from these trends. No inclusions that have suffered from significant post-entrapment crystallization or beam or laser overlap on plagioclase are included here.

Table 3
Trace element concentrations of plagioclase-hosted melt inclusions from sample Plume5 D53-1 (all values in ppm weight)

Crystal	Inclusion	Rb (ppm)	Sr (ppm)	Y (ppm)	Zr (ppm)	Nb (ppm)	Ba (ppm)	La (ppm)	Ce (ppm)	Pr (ppm)	Nd (ppm)	Sm (ppm)
2	1	b.d.	134	18.5	63.1	b.d.	27.6	2.64	9.09	1.61	5.77	b.d.
2	6	b.d.	151	27.7	79.8	**2.2**	20.1	2.95	9.93	1.73	8.22	*1.80*
2	16	b.d.	129	21.2	61.6	*2.88*	25.4	3.35	7.95	1.76	6.80	2.10
3	1	b.d.	103	17.7	32.8	b.d.	14.6	2.15	6.02	0.85	5.28	2.35
4	1	b.d.	136	24.3	67.0	b.d.	37.7	2.71	7.96	1.62	6.94	*3.35*
4	12	b.d.	126	20.2	65.4	*2.06*	27.7	3.08	7.80	1.17	7.59	2.40
5	1	b.d.	105	17.9	61.3	b.d.	22.2	4.35	8.67	1.26	5.39	b.d.
6	1	b.d.	130	22.3	66.3	b.d.	24.7	4.28	9.31	1.90	7.33	*2.96*
6	2	**2.4**	129	24.1	65.4	**2.0**	24.7	2.79	7.84	1.32	7.32	2.35
6	3	b.d.	129	22.9	66.7	3.40	24.0	3.43	8.43	1.16	8.24	1.64
6	4	b.d.	137	20.2	78.2	b.d.	25.4	3.82	8.33	1.17	6.63	*2.19*
6	5	b.d.	121	22.0	52.4	b.d.	22.1	2.38	6.52	1.60	8.62	*2.78*
7	1	b.d.	126	23.8	61.2	b.d.	21.1	2.58	8.33	1.40	5.85	2.89
7	2	b.d.	102	22.8	58.5	**3.8**	14.0	2.33	6.69	1.23	7.18	*2.84*
8	1	b.d.	117	20.5	45.5	b.d.	21.1	2.64	7.05	*1.06*	6.50	*3.85*
9	1	b.d.	134	18.0	46.8	b.d.	10.6	2.14	6.41	b.d.	*3.23*	b.d.
10	1	b.d.	111	20.5	40.6	b.d.	11.7	1.54	6.27	1.11	6.40	b.d.
11	1	b.d.	134	16.7	34.8	b.d.	20.7	2.09	6.99	1.00	5.96	1.96
12	1	b.d.	137	23.7	64.9	2.34	38.0	2.94	8.84	1.44	8.13	*3.68*
12	2	b.d.	123	20.0	62.4	*3.46*	33.3	3.39	8.97	1.65	9.15	3.26
13	1	b.d.	103	21.8	54.1	b.d.	8.2	2.04	6.04	1.17	5.80	3.10
14	1	b.d.	142	20.5	58.6	1.97	21.3	3.17	8.69	1.37	6.60	2.87
15	1	b.d.	134	6.7	**2.0**	b.d.	20.8	1.32	4.29	*0.59*	2.97	b.d.
15	5	b.d.	119	9.0	*3.5*	b.d.	15.0	*1.00*	3.22	*0.51*	2.68	b.d.
15	0	**1.4**	104	8.8	18.9	**0.3**	11.9	1.05	2.99	0.44	3.02	0.84
17	1	b.d.	105	23.2	58.2	*1.47*	13.3	2.35	6.95	1.14	6.33	2.63
18	1	b.d.	124	22.3	69.0	*2.41*	30.6	3.20	8.78	1.58	5.97	2.87
18	4	b.d.	109	23.7	62.2	b.d.	12.9	2.03	6.40	1.22	5.87	3.46
20	3	b.d.	135	23.2	69.2	b.d.	31.0	3.54	11.74	*1.21*	*4.64*	*2.81*
21	1	b.d.	103	19.0	50.7	b.d.	12.3	1.83	5.40	0.86	5.50	2.42
23	1	b.d.	117	23.9	43.9	b.d.	6.4	1.65	5.11	1.01	4.75	2.82
23	5	b.d.	96	22.8	50.2	b.d.	7.0	1.70	5.42	0.88	5.36	2.82
Detection limit			4	3	2	1.5	1	0.5	0.5	0.5	0.5	0.5

b.d. = below detection.
Numbers in italics are below the 6-sigma filter for acceptable data but higher than the 3-sigma detection limit.
Numbers in bold are slightly below the 3-sigma detection limit but are reported for the sake of discussion.

tion of some plagioclase-hosted inclusions is not unique to this basalt or this region, but commonly affects plagioclase phyric N-MORB.

HFSE-depleted inclusions in crystal #15 may have slightly higher Al and lower Fe contents than most other inclusions in this sample, but any trend is masked by small changes related to post-entrapment crystallization. N-MORB inclusions that were heated (rehomogenized) in an earlier study by Sours-Page et al. (1999) to erase the effects of post-entrapment crystallization showed good trends of decreasing FeO and increasing Al_2O_3 and MgO contents as TiO_2 decreased to very low values.

The composition of the plagioclase that hosts the HFSE-depleted inclusions (An_{83}) falls well within the range of plagioclase crystals that host undepleted inclusions. The inclusions in crystal #15 (the crystal with the greatest number of HFSE-depleted inclusions) are no different in terms of their size and appearance than those of other crystals, although the density of inclusions in

Eu (ppm)	Gd (ppm)	Tb (ppm)	Ho (ppm)	Tm (ppm)	Yb (ppm)	Lu (ppm)	Hf (ppm)	Ta (ppm)	Pb (ppm)	Th (ppm)	U (ppm)	Spot size (μm)
0.98	3.26	0.57	*0.83*	0.29	1.90	0.35	1.42	*0.22*	b.d.	*0.16*	b.d.	30
1.40	3.53	0.57	0.99	0.36	2.92	0.37	2.45	*0.13*	0.60	0.21	0.09	50
1.31	4.20	0.62	0.80	0.33	2.03	0.32	1.64	*0.13*	0.75	0.21	b.d.	50
0.86	2.31	0.47	0.67	0.31	2.05	0.27	0.92	b.d.	0.38	0.11	b.d.	50
1.17	3.39	0.65	*0.66*	*0.32*	2.21	*0.28*	*1.64*	*0.14*	b.d.	*0.19*	b.d.	30
1.19	3.40	0.53	0.75	0.30	2.12	0.38	1.47	*0.11*	0.53	0.21	*0.04*	50
0.85	*2.63*	*0.41*	b.d.	0.31	2.42	*0.32*	*1.54*	b.d.	*0.50*	0.23	0.11	30
b.d.	*2.75*	0.70	0.85	0.29	2.13	0.39	1.70	b.d.	1.44	0.48	*0.21*	30
1.42	3.23	0.71	0.94	0.30	2.58	0.35	1.77	b.d.	0.57	0.17	b.d.	65
1.23	3.71	0.72	0.81	0.43	2.48	0.38	2.07	0.22	0.53	0.24	b.d.	50
1.09	4.53	0.58	*0.87*	0.52	3.16	0.61	*2.27*	b.d.	b.d.	b.d.	b.d.	30
0.97	3.24	0.66	*0.50*	b.d.	2.58	0.39	1.47	b.d.	*0.52*	0.31	*0.10*	30
0.80	3.22	0.52	0.97	*0.35*	2.55	0.30	1.35	*0.10*	b.d.	0.27	b.d.	30
1.37	*2.67*	0.61	1.03	*0.29*	1.56	0.47	1.66	b.d.	*0.77*	*0.12*	*0.10*	30
1.25	*3.12*	0.65	*0.72*	*0.30*	2.36	b.d.	*1.28*	*0.11*	*0.62*	b.d.	b.d.	30
0.78	*3.60*	0.63	0.88	*0.22*	2.62	0.37	*1.29*	*0.19*	*0.73*	0.37	b.d.	30
b.d.	*1.70*	*0.30*	0.84	0.29	2.35	*0.21*	b.d.	b.d.	*0.53*	b.d.	b.d.	30
1.04	b.d.	0.42	0.69	b.d.	1.82	0.26	1.31	b.d.	*0.58*	0.29	*0.09*	65
1.41	4.33	0.63	0.92	0.41	2.71	0.36	2.03	0.10	0.76	0.22	0.06	65
1.07	2.74	0.63	0.69	0.33	2.36	0.34	2.01	*0.18*	*1.22*	0.19	0.13	65
1.30	b.d.	0.69	0.98	0.33	2.39	0.34	1.87	b.d.	1.23	*0.12*	*0.08*	30
1.41	3.53	0.55	0.90	0.32	2.29	0.28	1.63	0.11	0.72	0.23	0.09	30
b.d.	b.d.	*0.22*	b.d.	b.d.	0.87	b.d.	b.d.	b.d.	1.20	*0.11*	b.d.	30
0.86	b.d.	*0.21*	b.d.	0.20	0.89	b.d.	b.d.	b.d.	*0.74*	0.08	b.d.	30
0.86	1.05	0.24	0.32	0.15	1.07	0.13	0.53	**0.02**	0.49	0.03	0.02	65
1.13	3.14	0.62	0.78	0.34	2.49	0.37	1.66	0.09	0.47	0.13	0.04	65
1.16	3.02	0.55	0.93	0.31	2.67	0.34	1.81	0.18	0.46	0.20	0.12	50
0.86	3.88	0.58	0.83	0.27	2.40	0.40	1.20	*0.07*	0.65	*0.09*	*0.05*	50
0.99	4.60	b.d.	0.78	*0.30*	1.88	0.47	2.91	b.d.	*0.72*	*0.14*	b.d.	30
1.02	3.07	0.44	0.77	0.26	1.85	0.31	1.25	b.d.	*0.31*	0.12	*0.05*	50
1.08	3.26	0.65	1.00	0.35	2.09	0.29	1.23	b.d.	0.54	0.11	b.d.	50
1.42	*3.04*	0.49	0.83	0.37	3.02	*0.31*	1.43	b.d.	*0.58*	0.16	*0.08*	30
0.5	0.5	0.5	0.5	0.5	0.5	0.5	1	0.2	0.5	0.1	0.08	30

this crystal is about the highest observed. There is no correlation between the size of the inclusion and the degree of HFSE depletion within any crystal. Because the crystals are only fragments, it is not possible to determine if the degree of HFSE depletion is constant within a growth zone as reported for samples from the Gorda Ridge and the Juan de Fuca Ridge (Nielsen et al., 1995, 2000; Sours-Page et al., 1999).

In the next section, we discuss whether the inclusions are related to hydrous fluid transport, and faithfully record liquids that are present beneath the MOR, as proposed by Nielsen et al. (2000). Next, we examine an alternative hypothesis: that HFSE depletion is related to the inclusion formation process by diffusion phenomenon, such that these compositions do not represent geologically significant liquids. We have not attempted to model the HFSE depletion in terms of crystal–liquid equilibrium (e.g., any style of partial melting, magma mixing or crystallization) because these processes cannot account for the difference in behavior between elements with similar bulk crystal–liquid partition coefficients (e.g., Ba and U; K and La). In the last part of this section, we consider whether melt inclusions in olivine may also be affected by formation processes.

5.1. Formation of HFSE-depleted inclusions by melting of hydrated peridotite?

The Cl enrichment observed in some HFSE-depleted inclusions suggested to Nielsen et al. (2000) that a hydrous fluid was involved in their formation. The order of depletion in the inclusions, i.e., HFSE>REE>LILE. is broadly characteristic of the solubility characteristics of a hydrous fluid (Brenan et al., 1995; Kogiso et al., 1997), although there are some inconsistencies: for example, the very different behavior of Eu and Sr compared to the REE is not predicted. Nielsen et al. (2000) proposed that HFSE-depleted inclusions are unmodified representatives of unusual basaltic liquids that were present sporadically during evolution of the magma, but absent or very diluted in the final host magma. The liquids supposedly formed by melting of depleted, hydrothermally altered peridotite that had a trace element signature (high LILE, low HFSE) dominated by fluid-caused alteration. This is still a viable hypothesis, but there are several factors that cast some doubt on it, and suggest that alternative hypotheses should also be considered. Firstly, higher Cl contents are associated with *lower* HFSE, but LILE concentrations are about the same as in "normal" inclusions. Thus, there is no correlation between LILE and Cl, as might be expected if the hydrous fluid was transporting these elements. This would require that the fluid-altered peridotite coincidentally produces melts with the same LILE contents as melts from fertile peridotite.

Secondly, the correlation between Cl enrichment and HFSE depletion in individual inclusions from a single sample (data from Nielsen et al., 2000) is not easily explained by such a process. Inclusions with very high Cl (e.g., 300 ppm) are the most HFSE-depleted, but inclusions with much lower Cl (32 ppm) show most of the HFSE depletion.

Thirdly, the level of Cl enrichment in HFSE-depleted inclusions from different samples is very variable. In the samples of this study, Cl enrichment is barely measurable, despite strong HFSE depletion. In other samples (Nielsen et al., 2000), Cl is much more enriched. These differences are also seen in the host glasses. The Plume 5 D53-1 sample has low Cl and Cl/K, and its HFSE-depleted inclusions also have low Cl compared to many of the basalts studied by Nielsen et al. (2000). In general, the intensity of Cl and Cl/K enrichment for HFSE-depleted inclusions from a sample is roughly correlated with the extent of Cl enrichment in the host lavas, suggesting that whatever process causes the high Cl of the inclusions is expressed in the host lavas and vice versa. The fact that Cl enrichment in the host glasses is not accompanied by enrichment of LILE or depletion of HFSE suggests that whatever contributes Cl to the inclusions does not contribute significantly to the budget of other elements.

5.2. The role of diffusion in forming HFSE-depleted inclusions

The relationship of HFSE depletion with ionic field strength suggests that diffusion may play a role. Although diffusion rates in silicate liquids are not known for all elements, the quantity Z^2r_i (Z = ionic charge, r_i = ionic radius) is strongly negatively correlated with diffusion rates and is a useful parameter to track diffusion controlled element fractionation (Hoffman, 1980). There is a clear relationship between Z^2r_i and the depletion trends displayed by the low-Ti inclusions (Fig. 6). Elements with high Z^2r_i, which should diffuse slowly, are strongly depleted, consistent with an important role for diffusion in generating these compositions.

The depletion of HFSE however is opposite to what we would expect for a process in which slow-diffusing incompatible elements build up in the liquid boundary layer adjacent to a crystallization front. An obvious source of incompatible element depleted material is the plagioclase host itself. Physical models involving diffusion must somehow account for this depletion. We suggest that the HFSE-depleted melt inclusions may have formed by dissolution of feldspar to make a melt that was depleted in incompatible elements.

5.2.1. Plagioclase dissolution

The tendency for HFSE-depleted inclusions to have high Mg#s suggests that plagioclase host grains might have encountered magmas with higher temperature, which could promote their dissolution (the lack of any relationship between HFSE depletion and lower An content of plagioclase argues against it). If a plagioclase crystal was formed at depth and ascended isothermally while immersed in the liquid

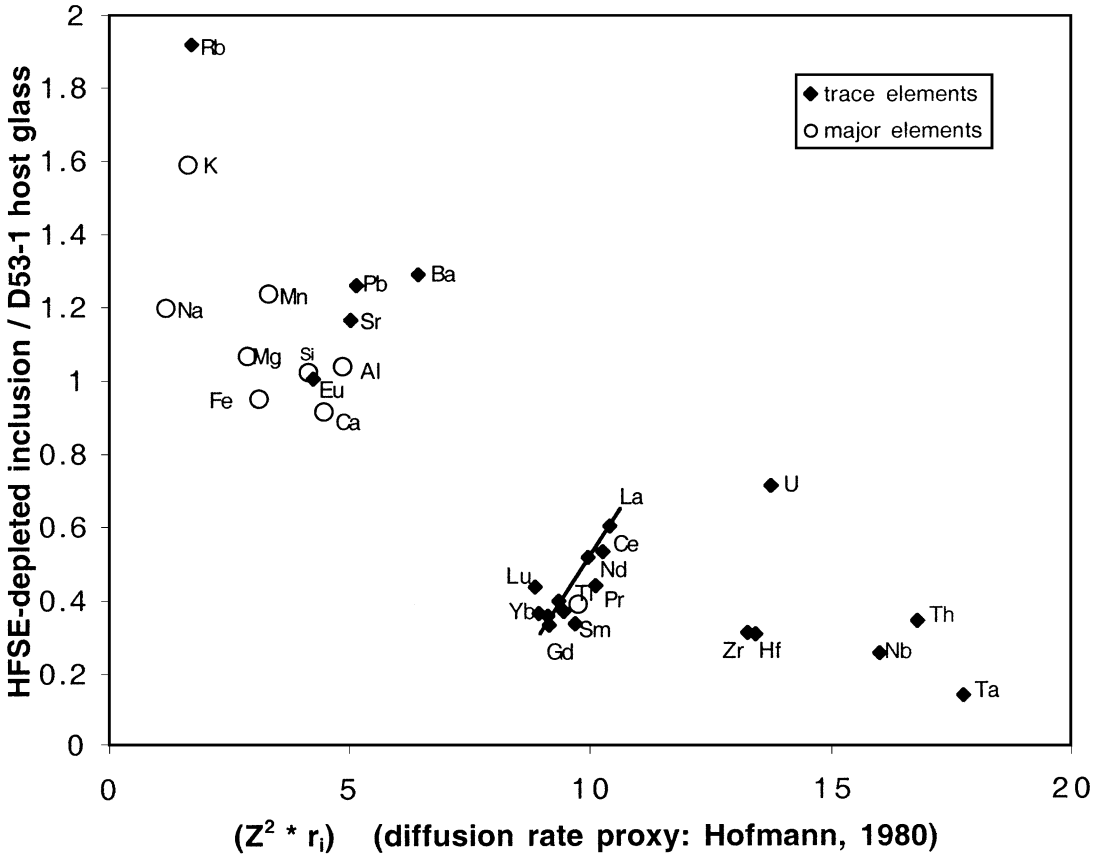

Fig. 6. Enrichment and depletion of a well-analyzed HFSE-depleted inclusion plotted vs. Z^2r_i, which tracks the diffusion rate in silicate liquids (Hofmann, 1980). Z (ionic charge) and r_i (ionic radius) are negatively correlated with diffusion rate in plagioclase, too (Giletti and Shanahan, 1997). Z and r_i are also related to fluid/solid partitioning. There is a good negative correlation of Z^2r_i with depletion. The small straight line shows the trend of the REE. Note also the relative enrichment of magmatically incompatible elements over less incompatible elements at the same Z^2r_i (e.g., La and Yb; U and Zr) suggesting that the host liquid was enriched in incompatible elements.

from which it formed, it should dissolve because of the positive pressure dependence of the plagioclase melting curve. It would also be more albitic than the equilibrium plagioclase for that liquid because of the negative pressure dependence of %An (about -1% An/kb (Fram and Longhi, 1992)).

Nakamura and Shimakita (1998) showed experimentally how plagioclase that was far out of chemical equilibrium (too sodic) with its hydrous host liquid dissolves at the head of a channel. Concomitantly, more calcic plagioclase reprecipitates on the channel walls behind, preventing mechanical mixing between the host liquid and the interior of the channel, and ultimately choking off the channel and forming a melt inclusion. Their modeling of this process shows how the concentrations of incompatible trace elements in the inclusion would be initially very low, similar to those in the feldspar. Under conditions where a reaction front in the channel advances rapidly, diffusion cannot keep up and elements with low diffusivity are depleted. Ultimately, the concentration of each element is determined by its ability to diffuse into the inclusion from the external basaltic melt, by its concentration in the external melt and by the speed at which the channel advances.

A similar model may be applicable to HFSE-depleted inclusions in MORB, although the conditions are quite different from the experiments. We note that Zr diffuses slowly and would take much longer to reach equilibrium concentration levels than faster dif-

fusing LIL elements like Ba, Rb and K. It is not clear that the channelized melting that Nakamura and Shimakita (1998) describe can occur under these relatively dry conditions, unless the feldspars were far from chemical equilibrium. Also, the shape and appearance of the natural HFSE-depleted inclusions in our MORB is unlike the inclusions created in Nakamura and Shimakita's (1998) experiments. Our inclusions more closely match what is produced experimentally using crystal and liquid compositions that are more appropriate to MORB, and only slightly out of chemical equilibrium (Nielsen et al., in preparation). However, the inclusions in these latter experiments do not form as channels and are not restricted from communicating with the host liquid, so they have the same composition as the host liquid and are not HFSE-depleted. To date, we have been unable to experimentally create HFSE-depleted inclusions in this system that look like the natural inclusions. It is clear that more experimental work needs to be done to address this issue.

A potential problem with Nakamura and Shimakita's (1998) mechanism for these basalts is the rate at which it must occur. If element concentrations are controlled by plagioclase dissolution accompanied by diffusion through melt channels as described above, then inclusions must be formed and isolated very rapidly (a matter of minutes or hours) because diffusion rates, even for HFSE, are rapid in silicate liquids (LaTourette et al., 1996). Using published diffusion coefficients for haplobasalt, (LaTourette et al., 1996) and the relationship $x=(Dt)^{1/2}$, Zr can diffuse approximately 11 μm in 1 min and 85 μm in 1 h at 1200 °C (x = diffusion distance, D = diffusion coefficient, t = time). Diffusion through a constricted pathway (e.g., a channel in plagioclase) is slower, but not by an order of magnitude (Watson, personal communication). For comparison, plagioclase dissolution rates are about 50 μm in 1 h, when the plagioclase is 50 °C out of equilibrium (Tsuchiyama, 1985). Such rapid processes seem geologically unlikely but are not inconceivable as crystals encounter changing conditions during magma movement through the crust.

5.2.2. Diffusion through plagioclase

Other processes that could lead to the formation of HFSE-depleted inclusions involve diffusion through plagioclase. If an inclusion that was depleted in all incompatible elements was completely enclosed by solid plagioclase, then it is possible that diffusion from a later, more enriched host melt through a thin layer of solid plagioclase might have modified the incompatible elements' concentrations in the inclusion. (Gaetani and Watson (2000) demonstrated such a process for Mg and Fe in olivine-hosted melt inclusions). The original depleted inclusion may have formed rapidly by dissolution of plagioclase as described earlier, but it is more likely that it was trapped as an ultradepleted melt similar to those in olivine (Sobolev, 1996; Sobolev and Shimizu, 1992) (see below). Diffusion rates in crystalline plagioclase are inversely related to Z and r_i (Gileti and Casserly, 1994; Giletti and Shanahan, 1997; LaTourette and Wasserburg, 1998; Cherniak and Watson, 1992) at least for monovalent and divalent cations, and possibly for higher valency cations as well. The dependence on r_i is especially strong (LaTourette and Wasserburg, 1998).

Re-equilibration of melt inclusions via diffusion through the crystal is a function of several factors in addition to time and diffusion rate. The size of the inclusion relative to the thickness of the crystal layer and the crystal–liquid partition coefficient also play a role (Qin et al., 1992). Using the formulations of Qin et al. (1992): for an inclusion that is 10 μm in diameter located 100 μm from the crystal–liquid boundary, if Zr diffuses in plagioclase at 10^{-14} cm^2/s, and has a partition coefficient of 0.001 (Fujimaki and Tatsumoto, 1984), then it would re-equilibrate $<2\%$ in 10 years. On the other hand, K with a diffusion rate of $10^{-11.5}$ (Giletti and Shanahan, 1997) and a partition coefficient of 0.3 (Higuchi and Nagasawa, 1969) would require less than a year to completely re-equilibrate for the same conditions. Thus, starting with an inclusion that was depleted in all incompatible elements, diffusion through plagioclase could create a trend similar to that seen in Fig. 6. It would require time scales on the order of years, which may be more reasonable than the melt diffusion mechanism described above. The lack of a relationship between inclusion size and HFSE depletion in this study argues against such a process, but does not eliminate it.

5.2.3. Cl enrichment and the melting/diffusion model

A model incorporating diffusion must also account for the Cl enrichment seen in some HFSE-depleted inclusions. We note that the lack of concomitant

fluorine enrichment in high-Cl, HFSE-depleted inclusions (Nielsen, unpublished data) shows that this Cl enrichment is not directly related to diffusion (e.g., of anions to maintain charge balance). It is more likely that the Cl is supplied by a hydrous fluid (Nielsen et al., 2000).

It is possible that plagioclase crystals encountered Cl-rich regions in a magma chamber which had been contaminated by stoping of crust that contained a fluid or brine (Michael and Schilling, 1989; Michael and Cornell, 1998). To what extent might the $H_2O + Cl$ enriched magma have promoted the dissolution of plagioclase since the feldspar dissolution temperature is strongly dependent on pH_2O? Additional H_2O also results in a more anorthitic plagioclase. A 2-5 fold increase in the Cl content of these inclusions (i.e., up to 80 ppm) like we see here requires a 0.015–0.05 wt.% increase in H_2O if brine was the source, depending on the salinity of the brine. Addition of such a small amount (0.05 wt.%) of H_2O lowers stability of plagioclase by only about 5 °C (Housch and Luhr, 1991; Danyushvesky et al., 1996) and increases the An content by only about 0.2% An (Panjasawatwong et al., 1995). This is much less than the degree of disequilibrium in Nakamura and Shimakita's (1998) experiments. However, it is not clear how much disequilibrium is required to cause dissolution and how the rate of change of physical conditions influences the dissolution rate. The change does not seem sufficient to dissolve the feldspar, but may have allowed melting to proceed more quickly. The possibility of fluid involvement in the Cl-rich inclusions' formation should be tested further by analyses of stable isotope ratios and other indicators.

5.3. Incompatible element depletion in inclusions in olivine

The possibility that HFSE-depleted inclusions in plagioclase do not faithfully record their host liquid compositions raises some concern that ultradepleted inclusions in olivine also may have their initial melt compositions modified by these and comparable entrapment processes. Therefore, we ask if the present compositions of olivine-hosted inclusions reflect faithfully the magmatic component available on scales greater than these micron scales.

At first glance, the HFSE-depleted inclusions in plagioclase appear similar to the ultradepleted inclusions in olivine, which also have strongly depleted Ti and Zr contents (Sobolev and Shimizu, 1993) and very high Ti/Zr values. However, the ultradepleted inclusions in olivine are depleted in *all* incompatible elements, not just HFSE, and their sequence of depletion follows the order of bulk crystal–liquid partitioning. Unlike HFSE-depleted inclusions in plagioclase, the compositions of the olivine-hosted inclusions can be modeled by progressive fractional melting of a peridotite source (Sobolev, 1996; Sobolev and Shimizu, 1992; Shimizu, 1998). Alternative explanations are not required, but should be considered.

If the depleted melt inclusions in olivine were formed by a process of olivine dissolution with diffusion through melt as described in Section 5.2.1, then the depletion trends would be similar to those seen in plagioclase, so this mechanism can be discarded for the ultradepleted inclusions in olivine. If the depleted melt inclusions in olivine were formed by olivine dissolution followed by diffusion through later-crystallized olivine, the depletion trends would need to be related to olivine's diffusion rates, which are related to ionic radius (Jurewicz and Watson, 1988) and charge, and to crystal–melt partitioning (Qin et al., 1992). Diffusion rates for Cr^{3+} and Ti^{4+} in olivine are much slower than divalent cations because their diffusion involves charge imbalance (Scowen et al., 1991). Diffusion rates for monovalent cations have not been determined, but may also be slow because of charge imbalance. If so, LILE might be depleted too and the trends generated by a diffusional process might be similar to what is observed in olivine-hosted inclusions. Additional diffusion data for olivine would allow better evaluation of this process. Still, it would be difficult to cause the separation of La^{3+} and Sm^{3+} that is observed in some inclusions by diffusion (Shimizu, 1998; Sobolev and Shimizu, 1993), so this mechanism also seems unlikely. For either of the scenarios described above, it should be noted that olivine is less susceptible than plagioclase to dissolution, including in the presence of H_2O. The final process that was considered for plagioclase-hosted inclusions in Section 5.2.3 starts with trapping of an ultradepleted melt, like those in olivine. In summary, the evidence suggests that ultra-

depleted inclusions in olivine are formed by processes involving crystal–liquid equilibria: probably melting (Sobolev, 1996; Sobolev and Shimizu, 1992; Shimizu, 1998), and not by diffusional processes. Nevertheless, such processes should be critically evaluated in any melt inclusion study. The differences between ultra-depleted inclusions in olivine vs. HFSE-depleted inclusions in plagioclase might reflect a greater ability of olivine to isolate its inclusions from diffusional re-equilibration (Sobolev, 1996).

6. Incompatible element enrichment with decreasing Mg#

The inclusions within all 20 crystals studied display a range of Mg#, from about 71 to 65, and are on average more primitive than the host glass (Mg# = 66.8). Inclusions within any single crystal define a very limited range of Mg# compared to the entire suite of inclusions (Fig. 7). The inclusions also display a large range of K_2O, Ba and REE contents (Fig. 7; Tables 2 and 3), and are on average more enriched in incompatible elements than the host glass. The range of enrichment within each individual crystal is smaller than the range in the suite of inclusions as a whole. The fact that the inclusions bracket the host lava in terms of incompatible element enrichment and Mg# shows that liquids like these could have mixed to have formed the host lava, as proposed for other MORB (Sobolev, 1996; Sobolev and Shimizu, 1992; Sours-Page et al., 1999). However, the proportions of enriched and depleted inclusions are not representative of what is needed to form the bulk composition.

Once the HFSE-depleted inclusions are removed from consideration, it becomes apparent that all incompatible element concentrations increase with decreasing Mg#. As Mg# decreases from 71 to 65,

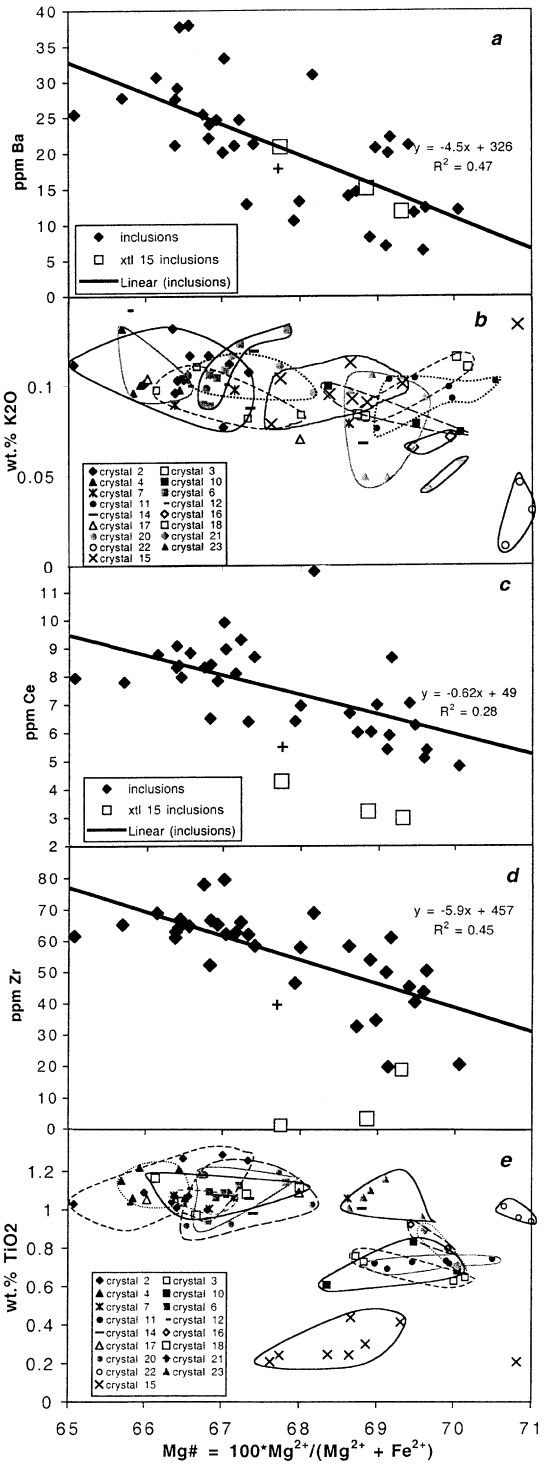

Fig. 7. Variation of incompatible elements with Mg#. Mg# = 100 × molar $Mg/(Mg+Fe^{2+})$, where $Fe^{2+} = 0.9 \times Fe_{total}$. Symbols as in Fig. 2, except for K_2O and TiO_2, where a different symbol is used for each crystal's inclusions to illustrate the limited range of variation in each crystal's inclusions. In the Ba, Ce and Zr diagrams, the best fit line that is shown (along with its slope and intercept and R^2) includes all diamond patterns, including a few mildly HFSE-depleted points.

Ba increases by a factor of 4, K_2O by a factor of 3, Ce by a factor of 1.8, Zr by a factor of 1.6, Sr by a factor of 1.5 and TiO_2 by a factor of 1.3. Based on major element modeling (Weaver and Langmuir, 1990), inclusions with the highest Mg#s (70–71) could be related to those with the lowest Mg#s (65–66) by about 15% crystallization. Thus, the amount of increase of incompatible elements with decreasing Mg# is greater than can be accounted for by fractional crystallization (Fig. 7). Furthermore, the order of over-enrichment (i.e., the increase of incompatible elements in a suite of liquids, over and above that generated by fractional crystallization alone) is the same as the order of bulk incompatibility during mantle melting. The form and order of over-enrichment is very similar to the enigmatic over-enrichment trends displayed by several suites of MORB lavas, including the FAMOUS suite (Bryan et al., 1979; Langmuir et al., 1977, 1992) and the EPR at 21°N (Hekinian and Walker, 1987). Similar trends were also described by Sours-Page et al. (1999), although the order of over-enrichment was masked by HFSE depletion. The process by which elements are over-enriched in melts is not well understood. The fact that the over-enrichment trends in the inclusions are in the same order as crystal–liquid partitioning, and are similar to the trends observed in the lavas, is strong evidence that the trends are related to a large-scale magmatic processes and not to a smaller scale diffusion effect.

It is important to look for correlations between enrichment and the physical characteristics of the inclusions as well. No correlations are seen between host plagioclase composition and the inclusions' Mg#s or incompatible element enrichment of inclusions or the inclusion density, unlike other studies (Sours-Page et al., this volume). No correlations are seen between the size, appearance, composition or density of inclusions either within individual crystals or between crystals in the suite as a whole (however, patchy inclusions were not analyzed).

The degree of increase of Sr with decreasing Mg# is similar to that of Nd, but less than that of Ce or Pr. This rules out crystallization of a phase assemblage that included large amounts of plagioclase (Langmuir et al., 1992) in generating the over-enrichment trends. It is more likely that these trends were caused by differences in source composition or melting.

Along ridge segments displaying over-enrichment in lavas (Bryan et al., 1979; Hekinian and Walker, 1987) more fractionated, over-enriched lavas are often found at some distance from the central axis while primitive lavas are found on the central axis. The temporal and spatial relationships between the diverse liquids cannot be constrained very well using the lavas. The presence of a large range of Mg#s and accompanying over-enrichment in the inclusions of a single sample indicates that the diverse liquids occur together in time and space. They also suggest that individual samples may frequently be formed as mixtures of these diverse liquids, even when their host glasses do not themselves display over-enrichment trends.

6.1. Incompatible element enrichment and HFSE-depleted lavas

Signs of incompatible element enrichment are also present in HFSE-depleted inclusions. The effects of whatever process causes HFSE depletion can be compensated for by comparing elements with similar Z^2r_i but different magmatic partitioning. For example, HFSE-depleted inclusions have LREE that are enriched relative to MREE and HREE, and therefore higher La/Sm than the host glass (Fig. 6). Other inclusion/host comparisons in Fig. 6 (Ba>Ca; U>Zr; Rb>K>Na) also suggest that the host liquid involved in forming the HFSE-depleted inclusions was actually incompatible element enriched. This is not surprising since many of the inclusions that are not HFSE-depleted are enriched in incompatible element concentrations and La/Sm ratios compared to the host basalt. This is further evidence that the process of HFSE depletion is preceded by whatever process produces variably enriched liquids.

7. Conclusions

A small but significant proportion of plagioclase-hosted melt inclusions in phyric MORB display depletions in incompatible elements that are related to the ion's field strength. HFSE are strongly depleted, while REE are moderately depleted and LILE are not depleted compared to the plagioclase' host glass. The depletions could not have been caused by crystal–

liquid equilibrium processes since elements with similar bulk distribution coefficient behave very differently. An earlier hypothesis for this phenomenon (Nielsen et al., 2000), that the liquids were formed by melting of hydrothermally altered depleted peridotite, does not account for all of the chemical observations. We present alternative hypotheses that these inclusions obtained their distinctive HFSE depletion by diffusional processes related to inclusion formation. The degree of depletion is related to the quantity $Z^2 r_i$, which in turn tracks the diffusion rate in silicate magmas (Hofmann, 1980) and perhaps plagioclase as well. We suggest that one way HFSE-depleted inclusions may form is by rapid plagioclase dissolution to yield a plagioclase-rich melt. Incompatible elements diffuse into the inclusion from the host melt. The diffusion rate of each ion controls the degree of equilibration with the host melt. Diffusion could occur through melt channels if the process is very rapid, or through solid plagioclase if it is a much slower process. An alternative diffusion-related mechanism by which HFSE-depleted inclusions could form would involve entrapment of ultradepleted melt inclusions similar to those observed in olivine, followed by diffusion of incompatible elements from a later, more enriched host melt through solid plagioclase. In either case, the inclusions do not represent geologically significant liquids that are present in the magmatic system: their compositions do not provide unambiguous information about melting processes or source composition. Sporadic high Cl in the inclusions is possibly derived by hydrothermal contamination of the magmatic system and may have aided in plagioclase dissolution. Once these inclusion formation processes can be accounted for, other processes, such as mantle source composition, and melting can be examined more confidently. For example, it appears that most melt inclusions in this study formed from liquids that were incompatible element enriched compared to the current host basalt.

Acknowledgements

Many thanks to the organizers of the Melt Inclusion Symposium in Grenoble. Stimulating discussions there with Leonid Danyushevsky, Alex Sobolev, Al Hofmann, Charles Langmuir, Fred Anderson, Nobu Shimizu, Erik Hauri, and Dima Kamenetsky motivated this paper, even though it may not express their views. Discussions with Bruce Watson, Glenn Gaetani, and Jim Van Orman helped clarify how diffusion operates. Constructive reviews by Alexander Sobolev, James Van Orman and William Minarik significantly improved the paper. This work was supported by U.S. National Science Foundation (NSF) grants OCE 93 14483 and OCE 9811161 and an NSF Oklahoma EPSCoR grant.

References

Brenan, J.M., Shaw, H.F., Ryerson, F.J., Phinney, D.L., 1995. Mineral–aqueous fluid partitioning of trace elements at 900 °C and 2.0 Gpa: constraints on the trace element chemistry of mantle and deep crustal fluids. Geochim. Cosmochim. Acta 59, 3331–3350.

Bryan, W.B., Thompson, G., Michael, P.J., 1979. Compositional variation in a steady state zoned magma chamber: mid-Atlantic Ridge at 36°50′N. Tectonophysics 55, 63–85.

Cherniak, D.J., Watson, E.B., 1992. A study of strontium diffusion in K-feldspar, Na–K feldspar and anorthite using Rutherford Backscattering Spectroscopy. Earth Planet. Sci. Lett. 113, 411–425.

Danyushvesky, L.V., Sobolev, A.V., Dmitriev, L.V., 1996. Estimation of the pressure of crystallization and H_2O content of MORB glasses: calibration of an empirical technique. Mineral. Petrol. 57, 185–204.

Fox, P.J., Grindlay, N.R., Macdonald, K.C., 1991. Temporal and spatial variations of magmatic segments: the Mid-Atlantic Ridge (31°–34°30′S). Mar. Geophys. Res. 13, 1–20.

Fram, M.S., Longhi, J., 1992. Phase equilibria of dikes associated with Proterozoic anorthosite complexes. Am. Mineral. 77, 605–616.

Fujimaki, H., Tatsumoto, M., 1984. Partition coefficients of Hf, Zr and REE between phenocrysts and groundmass. Proc. Lunar Planet. Sci. Conf., 14th, Part 2, J. Geophys. Res. 89 (Suppl.), B662–B672.

Gaetani, G.A., Watson, E.B., 2000. Open system behavior of olivine-hosted melt inclusions. Earth Planet. Sci. Lett. 183, 27–41.

Giletti, B.J., Casserly, J.E.D., 1994. Strontium diffusion kinetics in plagioclase feldspars. Geochim. Cosmochim. Acta 58, 3785–3793.

Giletti, B.J., Shanahan, T.M., 1997. Alkali diffusion in plagioclase feldspar. Chem. Geol. 139, 3–20.

Grindlay, N.R., Fox, P.J., Macdonald, K.C., 1991. Second-order ridge axis discontinuities in the South Atlantic: morphology, structure and evolution. Mar. Geophys. Res. 13, 21–49.

Gurenko, A.A., Chaussidon, M., 1995. Enriched and depleted primitive melts included in olivine from Icleandic tholeiites: origin by continuous melting of single mantle column. Geochim. Cosmochim. Acta 59, 2905–2917.

Hekinian, R., Walker, D., 1987. Diversity and spatial zonation of

volcanic rocks from the East Pacific Rise near 21°N. Contrib. Mineral. Petrol. 96, 265–280.
Higuchi, H., Nagasawa, H., 1969. Partition coefficients of trace elements between rock forming minerals and their host volcanic rocks. Earth Planet. Sci. Lett. 7, 281–287.
Hofmann, A.W., 1980. Diffusion in natural silicate melts: a critical review. Physics of Magmatic Processes. Princeton Univ. Press, Princeton, NJ, pp. 385–417.
Housch, T.B., Luhr, J.F., 1991. Plagioclase–melt equilibria in hydrous systems. Am. Mineral. 76, 477–492.
Jarosewich, E., Nelen, J.A., Norberg, J.A., 1980. Reference samples for electron microprobe analysis. Geostand. Newsl. 4, 43–47.
Jurewicz, A.J.J., Watson, E.B., 1988. Cations in olivine: Part 2. Diffusion in olivine phenocrysts, with applications to peterology and mineral physics. Contrib. Mineral. Petrol. 99, 186–201.
Kogiso, T., Tatsumi, Y., Nakano, S., 1997. Trace element transport during dehydration processes in the subducted oceanic crust: 1. Experiments and implications for the origin of oceanic island basalts. Earth Planet. Sci. Lett. 148, 193–205.
Langmuir, C.H., Bender, J.F., Bence, A.E., Hanson, G.N., Taylor, S.R., 1977. Petrogenesis of basalts from the FAMOUS area: Mid-Atlantic Ridge. Earth Planet. Sci. Lett. 36, 133–156.
Langmuir, C.H., Klein, E.M., Plank, T., 1992. Petrological systematics of mid-ocean ridge basalts: constraints on melt generation beneath ocean ridges. In: Phipps Morgan, J., Blackman, D.K., Sinton, J.M. (Eds.), Mantle Flow and Melt Generation at Mid-Ocean Ridges, AGU, Geophys. Monograph, vol. 71, pp. 183–280.
LaTourette, T., Wasserburg, G.J., 1998. Mg diffusion in anorthite: implications for the formation of early solar system planetesimals. Earth Planet. Sci. Lett. 158, 91–108.
LaTourette, T., Wasserburg, G.J., Fahey, A.J., 1996. Self diffusion of Mg, Ca, Ba, Nd, Yb, Ti, Zr and U in haplobasaltic melt. Geochim. Cosmochim. Acta 60, 1329–1340.
Michael, P.J., Cornell, W.C., 1998. Influence of spreading rate and magma supply on crystallization and assimilation beneath mid-ocean ridges: evidence from chlorine and major element chemistry of mid ocean ridge basalts. J. Geophys. Res. 103, 18325–18356.
Michael, P.J., Schilling, J.-G., 1989. Chlorine in mid-ocean ridge magmas: evidence for assimilation of seawater-influenced components. Geochim. Cosmochim. Acta 53, 3131–3143.
Michael, P.J., Forsyth, D.W., Blackman, D.K., Fox, P.J., Hanan, B.B., Harding, A.J., Macdonald, K.C., Neumann, G.A., Orcutt, J.A., Tolstoy, M., Weiland, C.M., 1994. Mantle control of a dynamically evolving spreading center: Mid-Atlantic Ridge, 31°–34°S. Earth Planet. Sci. Lett. 121, 451–468.
Nakamura, M., Shimakita, S., 1998. Dissolution origin and syn-entrapment compositional change of melt inclusion in plagioclase. Earth Planet. Sci. Lett. 161, 119–133.
Nielsen, R.L., Crum, J., Bourgeois, R., Hascall, K., Forsythe, L.M., Fisk, M.R., Christie, D.M., 1995. Melt inclusions in high-An plagioclase from the Gorda Ridge: an example of the local diversity of MORB parent magmas. Contrib. Mineral. Petrol. 122, 34–50.
Nielsen, R.L., Sours-Page, R.E., Harpp, K.S., 2000. Role of a Cl-bearing flux in the origin of depleted ocean floor magmas. Geochem. Geophys. Geosyst. 1. Paper number 1999GC000017.
Panjasawatwong, Y., Danyushevsky, L.V., Crawford, A.J., Harris, K.L., 1995. An experimental study of the effects of melt composition on plagioclase–melt equilibria at 5 and 10 kbar: implications for the origin of magmatic high-An plagioclase. Contrib. Mineral. Petrol. 118, 420–432.
Pearce, N.J.G., Perkins, W.T., Westgate, J.A., Gorton, M.P., Jackson, S.E., Neal, C.R., Chenery, S.P., 1997. A compilation of new and published major and trace element data for NIST SRM 610 and NIST SRM 612 glass reference materials. Geostand. Newsl. 21, 115–144.
Pyle, D.G., Christie, D.M., Mahoney, J.J., Duncan, R.A., 1995. Geochemistry and geochronology of ancient southeast Indian and southwest Pacific seafloor. J. Geophys. Res. 100, 22261–22282.
Qin, Z., Lu, F., Anderson, A.T., 1992. Diffusive reequilibration of melt and fluid inclusions. Am. Mineral. 77, 565–574.
Rudnick, R.L., Barth, M.G., Horn, I., McDonough, W.F., 2000. Rutile-bearing refractory eclogites: missing link between continents and depleted mantle. Science 287, 278–281.
Scowen, P.A.H., Roeder, P.L., Helz, R.T., 1991. Reequilibration of chromite within Kilauea Iki lava lake, Hawaii. Contrib. Mineral. Petrol. 107, 8–20.
Shimizu, N., 1998. The geochemistry of olivine-hosted melt inclusions in a FAMOUS basalt ALV519-4-1. Phys. Earth Planet. Inter. 107, 183–201.
Sobolev, A.V., 1996. Melt inclusions in minerals as a source of principle petrological information. Petrology 4, 209–220.
Sobolev, A.V., Shimizu, N., 1992. Ultradepleted melts and the permeability of ocean mantle. Dokl. Akad. Nauk 326 (2), 354–360.
Sobolev, A.V., Shimizu, N., 1993. Ultra-depleted primary melt included in an olivine from the Mid-Atlantic Ridge. Nature 363, 151–154.
Sobolev, A.V., Shimizu, N., 1994. The origin of typical NMORB: the evidence from a melt inclusion study. Mineral. Mag. 58A, 862–863.
Sobolev, A.V., Hofmann, A.W., Nikogosian, I.K., 2000. Recycled oceanic crust observed in 'ghost plagioclase' within the source of Mauna Loa lavas. Nature 404, 986–990.
Sours-Page, R., Johnson, K.T.M., Nielsen, R.L., Karsten, J.L., 1999. Local and regional variation of MORB parent magmas: evidence from melt inclusions from the Endeavour Segment of the Juan de Fuca Ridge. Contrib. Mineral. Petrol. 134, 342–363.
Tsuchiyama, A., 1985. Dissolution kinetics of plagioclase in the melt of the system diopside–albite–anorthite, and origin of dusty plagioclase in andesites. Contrib. Mineral. Petrol. 89, 1–16.
Weaver, B.L., 1991. Trace element evidence for the origin of ocean island basalts. Geology 19, 123–126.
Weaver, J.S., Langmuir, C., 1990. Calculation of phase equilibrium in mineral–melt systems. Comput. Geosci. 16, 1–19.